This article has been accepted for publication in a future issue of this journal, but has not been fully edited. Content may change prior to final publication. Citation information: DOI 10.1109/TMAG.2021.3121200, IEEE Transactions on Magnetics

An Adaptive Minimum-Frame-Error Rate Detector for Magnetic Recording

Shanwei Shi and John R. Barry, *Senior Member, IEEE*
School of Electrical and Computer Engineering, Georgia Institute of Technology, Atlanta, GA 30332 USA

A magnetic recording read channel has numerous parameters that must be carefully tuned for best performance; these include not only the equalizer coefficients but also any parameters inside the soft-output detector, some of which may be pattern dependent, including signal levels, predictor coefficients, and residual noise variances. Conventional tuning strategies based on a minimum-mean-squared error criterion are not optimal in terms of frame-error rate and ultimately areal density. Here we propose a strategy for optimizing the parameters with the aim of minimizing the frame-error rate after error-control decoding. The proposed strategy exploits the close connection between the frame-error rate and the gap between the two curves in an extrinsic information transfer chart. A stochastic gradient algorithm applied to a cost function that quantifies this gap leads to our proposed *adaptive minimum-frame-error rate (AMFER)* algorithm for adapting the equalizer and detector parameters. Numerical results based on a quasi-micromagnetic simulated channel show that the AMFER parameters can reduce the frame-error rate by more than two orders of magnitude, leading to a 7% gain in areal density over conventional MMSE parameters.

***Index Terms*—Soft-output detection, turbo processing, extrinsic information transfer (EXIT) chart.**

I. Introduction

THE exploding demand for cloud storage [1] is motivating a push for higher areal densities, with narrower track pitches and shorter bit lengths. The resulting increase in interference and media noise requires improvements in read channel signal processing to keep pace. A widely used technique for mitigating media noise is pattern-dependent noise prediction (PDNP) [2, 3]; in this approach, each bit pattern has its own set of parameters for computing a branch metric. PDNP was extended to multitrack detection in [4].

The traditional strategy for choosing the read channel parameters (including the signal levels, noise predictor coefficients, and residual variances) is based on a minimum mean-square-error (MMSE) criterion, in part because it guarantees a closed-form solution and a single local minimum. However, MSE is not as relevant to the end user as other metrics such as bit-error rate (BER), frame-error rate (FER), and areal density. The adaptive minimum-bit-error rate (AMBER) algorithm for tuning the parameters to minimize BER instead of MSE was recently proposed [5, 6]; results showed that AMBER can provide a 20% decrease in BER and an 8% increase in areal density. In [7, 8], the parameters to reduce BER and computation time are estimated via deep neural networks.

The BER after detection, while more relevant than MSE, is still not as relevant to the end user as the FER after error-control decoding, because the FER is what ultimately determines areal density. In a state-of-the-art read channel, a soft-output detector and a soft-input error-control decoder work iteratively in a turbo fashion with soft information transferring between them. The soft-output detector is typically either the BCJR algorithm [9] or the soft-output Viterbi algorithm (SOVA) [10].

Techniques for analyzing the convergence of iterative decoding schemes have been widely studied. Density evolution for low-density parity-check (LDPC) codes was developed by tracking the probability distributions of extrinsic log-likelihood ratios (LLR's) [11]. This tracking is simplified considerably when the probability density function (PDF) depends on only a single parameter. Other single-parameter metrics include the fidelity of [12] and the mutual information of [13]. In [13], Ten Brink developed the *extrinsic information transfer (EXIT)* chart to visualize the evolution of LLR's and analyze the convergence behavior. Prior work regarding EXIT charts has been limited to the design of error-control codes [14]–[16], not detectors.

In this paper, we propose a cost function for optimizing the detector parameters based on an EXIT chart. By choosing detector parameters to minimize this cost function, the FER can be dramatically reduced. We develop an adaptive algorithm for tuning the parameters of the equalizer and detector aiming to minimize FER. We apply the algorithm to a SOVA detector, and test it on both a simple intersymbol interference (ISI) channel and a more realistic set of simulated magnetic recording channel waveforms.

This paper is organized as follows. In Section II, we review EXIT charts. In Section III, we propose the minimum-FER tuning strategy and the AMFER algorithm. In Section IV, we evaluate the performance of the proposed algorithm, and compare it to traditional MMSE parameters. In Section V, we summarize this paper.

II. The EXIT Chart

We consider the magnetic recording read channel illustrated in Fig. 1 [17]. A vector $\mathbf{r}$ of readback waveform samples is fed to an equalizer, producing a vector $\mathbf{y}$ of equalizer outputs. An *a posteriori* probability (APP) detector has two inputs: the equalizer output $\mathbf{y}$, and a vector $\boldsymbol{\lambda}_2 = [\lambda_{2,0}, ..., \lambda_{2,N-1}]^T$ of *a priori* LLR's about the N written coded bits $\mathbf{a} = [a_0, ..., a_{N-1}]^T$, where $\lambda_{2,k} = \ln(\frac{P(a_k=1)}{P(a_k=0)})$. Based on these inputs, the APP detector estimates the vector $\mathbf{L} = [L_0, ..., L_{N-1}]^T$ of APP LLR's about the written coded bits, where $L_k = \ln(\frac{P(a_k=1|\mathbf{y})}{P(a_k=0|\mathbf{y})})$. The difference $\boldsymbol{\lambda}_1 = \mathbf{L} - \boldsymbol{\lambda}_2$ is a vector of *extrinsic* LLR's,

This article has been accepted for publication in a future issue of this journal, but has not been fully edited. Content may change prior to final publication. Citation information: DOI 10.1109/TMAG.2021.3121200, IEEE Transactions on Magnetics

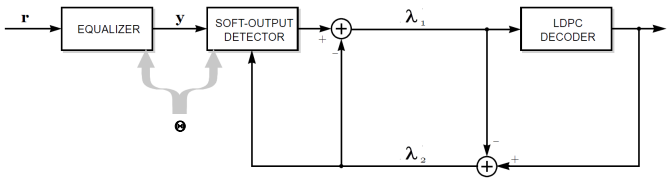

Fig. 1. A soft-output detector interacting with an LDPC decoder in an iterative (turbo) fashion.

which are fed as a priori information to the LDPC decoder. In a symmetric fashion, the LDPC decoder estimates the APP LLR's about the coded bits, which after subtracting the decoder a priori information leads to the vector $\boldsymbol{\lambda}_2$ of extrinsic information from the decoder. As shown in the figure, $\boldsymbol{\lambda}_2$ is then interpreted as a priori information by the detector in the next iteration. The detector and decoder thus work in an iterative (turbo) fashion until a coded frame is successfully decoded or a maximum iteration number is reached.

As indicated in Fig. 1, we use $\boldsymbol{\Theta}$ to denote all of the parameters to be optimized, including the equalizer coefficients and any parameters within the detector. For simplicity, Fig. 1 omits any interleavers that might be used to prevent burst errors.

A Gaussian distribution is characterized by two parameters, mean and variance. A Gaussian distribution is said to be *consistent* when the variance is twice the mean, and is thus characterized by a single parameter. Likewise, the *a priori* information $\boldsymbol{\lambda}_2$ is said to be *consistent* when the random variables $\{z_{2,k} = \lambda_{2,k}a_k\}$ are i.i.d. $\mathcal{N}(\mu_2, 2\mu_2)$ for some parameter μ_2. These random variables will be neither consistent nor independent in general; nevertheless (as recognized in [13]) they can be roughly approximated as such, and we will see that optimizing the detector is dramatically simplified when the a priori information coming from the decoder is assumed to be consistent.

The quality of the a priori LLR's is captured by the mutual information $I_2 \triangleq I(\{\lambda_{2,k}\}; \{a_k\})$ between the written bits and the a priori LLR's [13], which (under the consistent Gaussian approximation) reduces to (see the Appendix):

$$I_2 = 1 - E(\log_2(1 + e^{-Z_2})), \tag{1}$$

where $Z_2 \sim \mathcal{N}(\mu_2, 2\mu_2)$.

The mutual information $I_1 \triangleq I(\{\lambda_{1,k}\}; \{a_k\})$ after the detector will depend in a predictable way on the mutual information I_2 after decoding. Let

$$I_1 = T_1(I_2) \tag{2}$$

denote the function that relates I_2 to I_1; it is an increasing function that approaches $T_1(I_2) \to 1$ as $I_2 \to 1$. Similarly, let T_2 denote the function that relates I_1 to I_2:

$$I_2 = T_2(I_1). \tag{3}$$

The $T_1(\,\cdot\,)$ and $T_2(\,\cdot\,)$ functions are the so-called *extrinsic information transfer (EXIT)* functions. Given readback waveforms, the shape of T_1 is determined by the parameters of the equalizer and detector. Closed-form expressions for these transfer functions are unknown, they must be measured empirically. We simplify the calculation of T_2 by implementing a time-averaged version of (1), which strictly speaking only applies when $\{a_k\lambda_{2,k}\}$ are i.i.d. consistent Gaussian, even when they are not:

$$I_2 = 1 - \frac{1}{N}\sum_{k=0}^{N-1} \log_2(1 + e^{-a_k\lambda_{2,k}}). \tag{4}$$

Likewise, the mutual information between the extrinsic LLR's after the detector and the written bits can be estimated using:

$$I_1 = 1 - \frac{1}{N}\sum_{k=0}^{N-1} \log_2(1 + e^{-a_k\lambda_{1,k}}). \tag{5}$$

A chart showing both T_1 and T_2 is known as an EXIT chart, and is a powerful tool for understanding convergence of iterative detectors. We illustrate an EXIT chart with an example.

Example 1. Consider an ISI channel $H(z) = 0.5 + z^{-1} + 0.5z^{-2}$ with AWGN, and suppose the written bits are coded by a rate-$8/9$ LDPC code of length 16200 from DVB-S2 [18]. A five-tap equalizer and a two-tap partial-response monic target are jointly chosen according to the MMSE criterion, followed by a two-state SOVA detector. In Fig. 2 we plot the transfer function $T_1(I_2)$ versus I_2 for $\mathrm{SNR} = \sum_k h_k^2/(2\sigma_n^2)$ values of 6.7 dB, 6.3 dB, and 5.9 dB. Each curve is found by sweeping through all possible I_2 values, or equivalently through all possible μ_2 values, and for each one generate an artificial consistent Gaussian a priori vector $\boldsymbol{\lambda}_2 = \mu_2\mathbf{a} + \mathbf{w}_2$, where the components of $\mathbf{w}_2$ are i.i.d. $\mathcal{N}(0, 2\mu_2)$. After SOVA uses $\boldsymbol{\lambda}_2$ as a priori information to generate $\mathbf{L}$, the extrinsic information $\boldsymbol{\lambda}_1 = \mathbf{L} - \boldsymbol{\lambda}_2$ is used to estimate I_1 via (5). Improved estimates are found by averaging these I_1 values over repeated trials. Also shown in the figure is the transfer curve $T_2^{-1}(I_2)$ for the LDPC decoder, which is independent of SNR and is found in a symmetric way. For each possible μ_1 generate a consistent Gaussian a priori vector $\boldsymbol{\lambda}_1 = \mu_1\mathbf{a} + \mathbf{w}_1$, where the components of $\mathbf{w}_1$ are i.i.d. $\mathcal{N}(0, 2\mu_1)$. The extrinsic information $\boldsymbol{\lambda}_2$ is achieved by subtracting a priori information $\boldsymbol{\lambda}_1$ from the decoder outputs and is used to estimate I_2 via (4). As shown in the figure, the T_1 curve drops lower as the SNR decreases, and the two curves intersect when $\mathrm{SNR} = 5.9$ dB. The green dashed staircase curve shows a sample decoding trajectory for the case when $\mathrm{SNR} = 6.7$ dB. The trajectory starts at $(0,\ 0)$, bounces between the two transfer functions, and stops near $(1,\ 1)$, after the decoding is successful.

III. Adaptive Minimum-Frame-Error Rate Algorithm

A direct optimization of the parameters $\boldsymbol{\Theta}$ to minimize FER would require an analytical expression for FER in terms of the parameters to be optimized; such an expression is unknown and likely to be unwieldy even if it were known. Instead, we propose to indirectly optimize FER by optimizing the EXIT chart. It has been shown in [13] that when the curves in an EXIT chart intersect, there is a high probability of decoding failure. In contrast, a clear tunnel between the two curves means the decoding is very likely to be successful. The wider the tunnel is, the faster the convergence will be.

This article has been accepted for publication in a future issue of this journal, but has not been fully edited. Content may change prior to final publication. Citation information: DOI 10.1109/TMAG.2021.3121200, IEEE Transactions on Magnetics

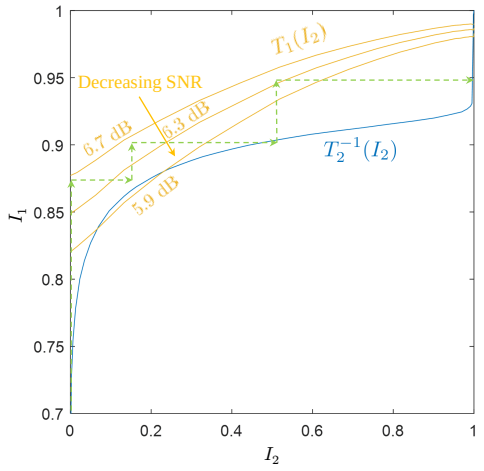

Fig. 2. EXIT chart for Example 1 under different SNR's.

Decoding success is not so much dependent on the entire shape of the two curves in an EXIT chart, but is instead determined largely by what the two curves look like when they are closest to each other. Motivated by this observation, and with the understanding that a larger gap between the two curves leads to a higher probability of decoding successfully and faster decoding, we propose to choose the parameters $\mathbf{\Theta}$ so as to maximize the gap between the two curves at a particular value I_2^* for I_2, where I_2^* is chosen in the "bottleneck" region of the chart where the two curves are closest. In the example of Fig. 2, a value of I_2^* around 0.2 would be an appropriate choice when $\text{SNR} = 5.9$ dB.

Since only the T_1 curve depends on $\mathbf{\Theta}$, maximizing the gap is equivalent to maximizing T_1. Exploiting (5), we propose to choose $\mathbf{\Theta}$ to minimize the following cost function:

$$J(\mathbf{\Theta}) = \frac{1}{N}\sum_{k=0}^{N-1} \log_2(1+e^{-a_k\lambda_{1,k}^*}), \tag{6}$$

where $\{\lambda_{1,k}^*\}$ are the extrinsic LLR's produced by the detector when it is fed with a consistent Gaussian a priori vector $\boldsymbol{\lambda}_2 = \mu_2^*\mathbf{a} + \mathbf{w}_2$, where the components of $\mathbf{w}_2$ are i.i.d. $\mathcal{N}(0, 2\mu_2^*)$, where μ_2^* is the value of μ_2 that leads to I_2^* in (1).

As a result, the cost function does not depend on any features of the decoder or of the code itself. The proposed cost function requires knowledge of the written bits, which can be viewed as a form of training.

By either enlarging the bottleneck or opening a tunnel in the EXIT chart, we enhance the probability that the decoding trajectory passes through the bottleneck region. In the end, the FER will decrease. We should point out that maximizing T_1 at one point I_2^* may cause the mutual information to degrade at other values of I_2; if this effect is undesirable one could swap different parameter sets for different I_2 values, so that the detector parameters would change from one iteration to the next.

Applying the stochastic gradient algorithm to $J(\mathbf{\Theta})$ leads to the *adaptive minimum-frame-error rate (AMFER)* algorithm for adapting the parameters $\mathbf{\Theta}$:

$$\mathbf{\Theta}_{k+1} = \mathbf{\Theta}_k + \frac{\alpha a_k}{1+e^{a_k\lambda_{1,k}^*}}\nabla_{\mathbf{\Theta}}\lambda_{1,k}^*, \tag{7}$$

where α is the step size. Note the factor $\alpha a_k/(1+e^{a_k\lambda_{1,k}^*})$ in (7) can be interpreted as a time-varying step size that is negligible when $a_k\lambda_{1,k}^*$ is large; only when $a_k\lambda_{1,k}^*$ is negative or small will the parameters change significantly.

The AMFER algorithm of (7) is general and can be applied to a wide range of detector and equalizer architectures. Here we present a concrete example based on a 2^μ-state SOVA detector, where the parameters $\mathbf{\Theta}$ to be optimized are the equalizer coefficients $\mathbf{c}$, the noise standard deviation σ, and the signal levels $s(\mathbf{a}_k)$ associated with each bit pattern $\mathbf{a}_k = [a_k, ..., a_{k-\mu}]^T$. SOVA estimates the extrinsic LLR for a_k using:

$$\lambda_{1,k}^* = \hat{a}_k\Delta_k - \lambda_{2,k}, \tag{8}$$

where $\hat{a}_k$ is the bit chosen by the detector, Δ_k is chosen from a path metric margin M_k after time k (see Algorithm 1), and where the path metric margin M_k is the difference between the survivor path metric and the competing path metric:

$$\begin{aligned} M_k &= \sum_{i=0}^{\ell_k-1} -\log P(\bar{a}_{k-i}) + \frac{(\mathbf{c}^T\mathbf{r}_{k-i} - s(\bar{\mathbf{a}}_{k-i}))^2}{2\sigma^2} \\ &\quad - \sum_{i=0}^{\ell_k-1}(-\log P(\hat{a}_{k-i}) + \frac{(\mathbf{c}^T\mathbf{r}_{k-i} - s(\hat{\mathbf{a}}_{k-i}))^2}{2\sigma^2}) \\ &= \sum_{i=0}^{\ell_k-1}\frac{\hat{a}_{k-i}-\bar{a}_{k-i}}{2}\lambda_{2,k-i} + \frac{1}{2\sigma^2}(2\mathbf{c}^T\mathbf{r}_{k-i}(s(\hat{\mathbf{a}}_{k-i}) \\ &\quad - s(\bar{\mathbf{a}}_{k-i})) + s^2(\bar{\mathbf{a}}_{k-i}) - s^2(\hat{\mathbf{a}}_{k-i})), \end{aligned} \tag{9}$$

where ℓ_k is the separation length of the two paths, and $\bar{a}_k$ is the competing bit. Plugging (9) and (8) into the AMFER algorithm (7), along with the relationship between M_k and Δ_k described in Algorithm 1, leads to the following update equations for the parameters $\mathbf{\Theta}$:

$$\begin{aligned} \mathbf{c}_{k+1} &= \mathbf{c}_k + \frac{a_k\hat{a}_k}{1+e^{a_k\lambda_{1,k}^*}}\sum_{i=0}^{\ell_k-1}\frac{\mathbf{r}_{k-i}}{\sigma^2}(s(\hat{\mathbf{a}}_{k-i}) - s(\bar{\mathbf{a}}_{k-i})), \\ \sigma_{k+1} &= \sigma_k - \frac{a_k\hat{a}_k}{1+e^{a_k\lambda_{1,k}^*}}\sum_{i=0}^{\ell_k-1}\frac{1}{\sigma^3}(2\mathbf{c}^T\mathbf{r}_{k-i}(s(\hat{\mathbf{a}}_{k-i}) \\ &\qquad - s(\bar{\mathbf{a}}_{k-i})) + s^2(\bar{\mathbf{a}}_{k-i}) - s^2(\hat{\mathbf{a}}_{k-i})), \\ &\text{for each } i \in \{0,1,...,\ell_k-1\}: \\ s(\hat{\mathbf{a}}_{k-i})_{k+1} &= s(\hat{\mathbf{a}}_{k-i})_k + \frac{a_k\hat{a}_k}{1+e^{a_k\lambda_{1,k}^*}}(\frac{\mathbf{c}^T\mathbf{r}_{k-i} - s(\hat{\mathbf{a}}_{k-i})}{\sigma^2}) \\ s(\bar{\mathbf{a}}_{k-i})_{k+1} &= s(\bar{\mathbf{a}}_{k-i})_k - \frac{a_k\hat{a}_k}{1+e^{a_k\lambda_{1,k}^*}}(\frac{\mathbf{c}^T\mathbf{r}_{k-i} - s(\bar{\mathbf{a}}_{k-i})}{\sigma^2}). \end{aligned} \tag{10}$$

A common modification in iterative detectors (see e.g. [7]) is to introduce an extra parameter that scales the LLR's after the detector and before the decoder. Instead of choosing this parameter based on an ad hoc search based on empirical results, as is commonly done, it can be folded into $\mathbf{\Theta}$ and optimized by AMFER.

This article has been accepted for publication in a future issue of this journal, but has not been fully edited. Content may change prior to final publication. Citation information: DOI 10.1109/TMAG.2021.3121200, IEEE Transactions on Magnetics

The pseudocode of a SOVA detector whose parameters are adapted according to the proposed AMFER algorithm is shown in Algorithm 1. Code lines 5 to 18 are the conventional SOVA detector, while lines 19 to 20 implement the AMFER algorithm.

IV. Quantitative Results

A. Linear ISI Example

In this subsection we continue the linear ISI channel of Example 1. We set the maximum number of decoder iterations to ten, and the maximum number of overall (turbo) iterations to twenty. For the training process, we train the parameters (the equalizer, signal levels and residual noise variance) with one frame of 16200 bits for 500 epochs. MMSE initials are used for the first epoch. In each epoch, we generate different a priori information and the step size is $\alpha = 10^{-5}$. The bottleneck point we try to break through is $I_2^* = 0.2$.

In Fig. 3 we compare MMSE and AMFER EXIT charts, when SNR $= 5.9$ dB. The red curve shows T_1 with AMFER parameters, while the orange curve shows T_1 with MMSE parameters. The blue curve shows T_2^{-1} for the LDPC decoder, which is independent of the parameters. From the figure we can see that in the case of MMSE parameters, the two curves intersect. On the other hand, in the case of AMFER parameters, there is a distinct gap near $I_2^* = 0.2$ between the T_1 curve and the T_2^{-1} curve. We also observe that although the AMFER curve is not superior to the MMSE curve when $I_2 > 0.6$, the ultimate FER is dramatically better; the FER with AMFER is 0.068, as opposed to an FER of 0.605 with MMSE.

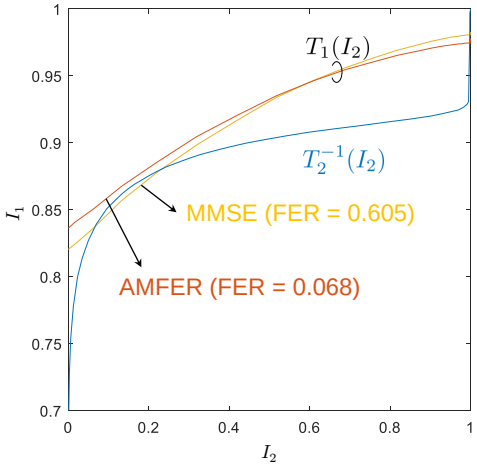

Fig. 3. EXIT chart with MMSE and AMFER parameters.

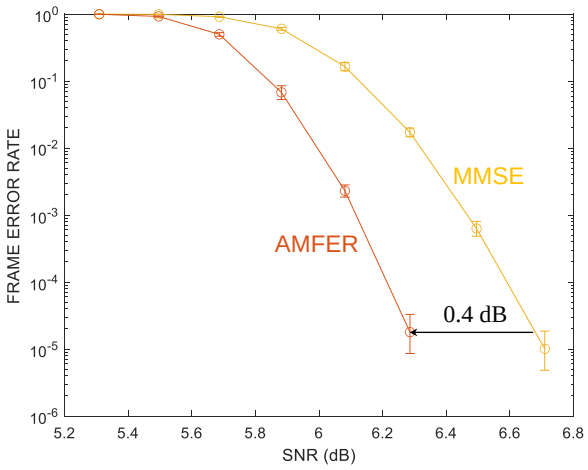

Fig. 4. FER vs SNR with MMSE and AMFER parameters.

In Fig. 4, we plot the FER versus SNR for both the MMSE and AMFER parameters. The error bars indicate the 95% confident interval. At around FER of 10^{-5}, the AMFER parameters outperform MMSE parameters by 0.4 dB.

Algorithm 1 A SOVA detector with parameters adapted by AMFER

Input: Equalizer input $\mathbf{y}$; I_2^*; initial values $s(\,\cdot\,)_0$, $\mathbf{c}_0$ and σ_0; step size α; training bits $\{a_0, a_2, ..., a_{N-1}\}$; termination conditions.

Output: AMFER parameters $s(\,\cdot\,)$, $\mathbf{c}$ and σ.

1: Get μ_2^* from I_2^* by inverting (1)
2: **repeat**
3: generate $\boldsymbol{\lambda}_2 = \mu_2^* \mathbf{a} + \mathbf{w}_2$, where the components of $\mathbf{w}_2$ are i.i.d. $\mathcal{N}(0, 2\mu_2^*)$
4: Run Viterbi algorithm to get $\{\hat{a}_k\}$
5: $\Phi_0(0) = 0,\ \Phi_0(p) = \infty\ \forall p \neq 0$
6: **for** $k = 1$ to L **do**
7: **for** $q = 0$ to $Q - 1$ **do**
8: **for** $p \in$ predecessors(q) **do**
9: $p^* = \text{argmin}_p\{\Phi_k(p) + \gamma_k(p, q)\}$
10: $\Phi_{k+1}(q) = \Phi_k(p^*) + \gamma_k(p^*, q)$
11: $\pi_{k+1}(q) = p^*$
12: **if** q is the survivor state at time k **then**
13: Calculate M_k using (9)
14: $\Delta_k = \infty$
15: Trace back to get the competing bit subsequence $\{\bar{a}_k, ..., \bar{a}_{k-\ell_k+1}\}$
16: **for** $i = 1$ to $\ell_k - 1$ **do**
17: **if** $\hat{a}_{k-i} \neq \bar{a}_{k-i}$ and $\Delta_{k-i} > M_k$ **then**
18: $\Delta_{k-i} = M_k$
19: Restore previous update on parameters at stage $k - i$, if any
20: Update $\boldsymbol{\Theta}_k$ using (10)
21: **end if**
22: **end for**
23: **end if**
24: **end for**
25: **end for**
26: **end for**
27: **until** Termination conditions are satisfied

This article has been accepted for publication in a future issue of this journal, but has not been fully edited. Content may change prior to final publication. Citation information: DOI 10.1109/TMAG.2021.3121200, IEEE Transactions on Magnetics

B. Ehime waveforms

We tested our algorithm on simulated waveforms provided by Ehime University, which were produced by realistic head fields and a Voronoi medium with Stoner-Wohlfarth switching [19]. Five consecutive tracks were written in a shingled fashion. In each track, there are 40950 independent pseudorandom bits sequence and 128 bits preamble and postamble, respectively. A total of 900 readback waveforms were produced with a fixed bit length of 7.3 nm, track pitches from 16.1 nm to 26.1 nm in 2 nm increments, reader widths from 70% to 145% in 15% increments (relative to a nominal reader width, whose full-width at half-maximum (FWHM) of the reader sensitivity function is 20.8 nm), and 25 reader positions in one-eight of a track pitch increments, spanning from the second to the fourth tracks. The readback waveforms from different tracks were perfectly synchronized. Despite the fact that the waveforms were not created using an error-control encoder, we can still test the turbo detector of Fig. 1 through the use of coset leaders; an uncoded block $\mathbf{c}$ of written bits can be interpreted as a codeword in the coset code $\mathbf{c} \oplus \mathcal{C}$ for any linear code $\mathcal{C}$. We also consider the written bits are interleaved and thus an interleaver and a de-interleaver are applied in the system.

We used the first 16200 bits for training the AMFER parameters, and the following 24999 bits to measure FER. Because the codeword length 16200 is much shorter than 24999, we are able to test multiple codewords from a single waveform by looking at different segments of the waveform. In particular, we consider 8800 consecutive bits as different starting locations for 8800 different codewords, and these frames are used for estimating FER. To limit any correlation between consecutive frames, we apply independent electronic noise (with an electronic SNR value of SNR_e = 24.6 dB) to each frame.

We test the AMFER algorithm in two scenarios. For the first scenario, the detector is SOVA without any pattern-dependent noise predictor. We consider the case of ten equalizer coefficients and four signal levels. For the second scenario, the detector is SOVA with PDNP. We set ten equalizer coefficients and eight patterns. Each pattern has three parameters (one signal level, one residual noise variance and one noise predictor coefficient). The update equations can be obtained by plugging the PDNP path metric [2, 3] into (8) and applying AMFER algorithm. The AMFER parameters are initialized with MMSE parameters and $I_2^* = 0.3$.

We compare the EXIT charts for different schemes in Fig. 5, assuming the track pitch is 24.1 nm and a centered reader with 70% width. The dashed curves are for the detectors without PDNP, while the solid curves are for the PDNP detectors. The MMSE curves are orange, while the AMFER curves are red. Without PDNP, the MMSE detector achieves FER = 0.937, while the AMFER detector achieves FER = 0.212, an improvement by more than a factor of 4. With PDNP, the MMSE detector achieves FER = 0.805, while the AMFER detector achieves FER = 0.009, an improvement by more than a factor of 89.

The areal density advantage of the AMFER algorithm is illustrated in Fig. 6, where we plot FER versus track pitch for the case of a centered reader with 70% width. The legend in this figure is as same as that in Fig. 5. The horizontal distance between two curves translates to areal density gain at a given value of FER. From the figure we see that the areal density advantage of AMFER over MMSE is roughly 5% without PDNP, and it is roughly 7% with PDNP.

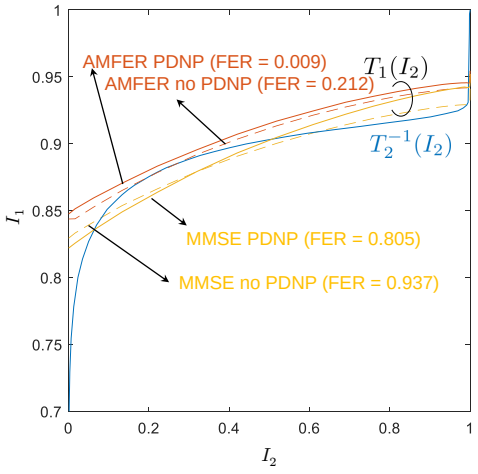

Fig. 5. EXIT chart from the Ehime waveforms.

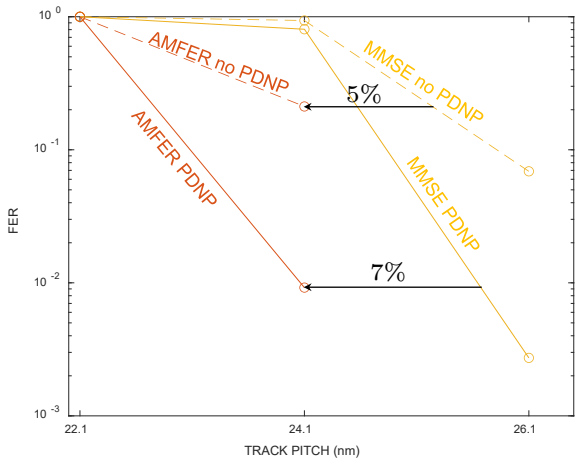

Fig. 6. FER versus track pitch with Ehime waveforms.

V. Conclusion

In this paper we propose a strategy for adapting the parameters of an equalizer and a soft-output detector so as to minimize the FER. The AMFER algorithm is general and applies to a wide range of detectors and read channels, including those using multiple readers and multitrack detection. For the case of single-track detection using PDNP SOVA and a single reader, numerical results using realistic readback waveforms show that the parameters found by the AMFER algorithm can lead to dramatic improvements in FER and areal density compared to MMSE parameters.

This article has been accepted for publication in a future issue of this journal, but has not been fully edited. Content may change prior to final publication. Citation information: DOI 10.1109/TMAG.2021.3121200, IEEE Transactions on Magnetics

APPENDIX
DERIVATION OF (1)

The mutual information between a discrete random variable $a \in \mathcal{A}$ and continuous random variable λ is

$$I = \sum_{a \in \mathcal{A}} \int_{-\infty}^{+\infty} P(a, \lambda) \log_2 \frac{P(\lambda|a)}{P(\lambda)} d\lambda.$$

When $P(a = -1) = P(a = 1) = 1/2$ and $P(\lambda|a) = \frac{1}{\sqrt{2\pi 2\mu}} e^{-\frac{(\lambda - a\mu)^2}{2(2\mu)}}$, I reduces to:

$$\begin{aligned} I &= \sum_{a \in \{-1,1\}} \int_{-\infty}^{+\infty} -P(a, \lambda) \log_2 \frac{1 + e^{-a\lambda}}{2} d\lambda \\ &= 1 - E(\log_2(1 + e^{-a\lambda})). \end{aligned}$$

ACKNOWLEDGMENT

This work was supported by IDEMA ASRC. The authors would like to thank Yasuaki Nakamura and Yoshihiro Okamoto from Ehime University, Japan, for providing the simulated waveforms, and also W. Radich, and F. Erden for their guidance and support.

REFERENCES

[1] D. Reinsel, J. Gantz, and J. Rydning, "The digitization of the world from edge to core," *Framingham: International Data Corporation*, 2018.
[2] A. Kavčić and J. M. Moura, "The Viterbi algorithm and Markov noise memory," *IEEE Trans. Inf. Theory*, vol. 46, no. 1, pp. 291–301, 2000.
[3] J. Moon and J. Park, "Pattern-dependent noise prediction in signal-dependent noise," *IEEE J. Sel. Areas Commun.*, vol. 19, no. 4, pp. 730–743, 2001.
[4] S. Shi and J. R. Barry, "Multitrack detection with 2D pattern-dependent noise prediction," in *Proc. IEEE Int. Conf. Commun. (ICC'18)*, 2018, pp. 1–6.
[5] ——, "Adaptive minimum-bit-error rate pattern-dependent noise prediction detection for magnetic recording," in *Proc. IEEE Int. Conf. Commun. (ICC'20)*, 2020, pp. 1–6.
[6] ——, "Minimum-bit-error rate tuning for PDNP detection," *IEEE Trans. Magn.*, vol. 57, no. 3, pp. 1–6, 2020.
[7] J. Shen, A. Aboutaleb, K. Sivakumar, B. J. Belzer, K. S. Chan, and A. James, "Deep neural network a posteriori probability detector for two-dimensional magnetic recording," *IEEE Trans. Magn.*, vol. 56, no. 6, pp. 1–12, 2020.
[8] A. Sayyafan, B. J. Belzer, K. Sivakumar, J. Shen, K. S. Chan, and A. James, "Deep neural network based media noise predictors for use in high-density magnetic recording turbo-detectors," *IEEE Trans. Magn.*, vol. 55, no. 12, pp. 1–6, 2019.
[9] L. Bahl, J. Cocke, F. Jelinek, and J. Raviv, "Optimal decoding of linear codes for minimizing symbol error rate (corresp.)," *IEEE Trans. Inf. Theory*, vol. 20, no. 2, pp. 284–287, 1974.
[10] J. Hagenauer and P. Hoeher, "A Viterbi algorithm with soft-decision outputs and its applications," in *Proc. IEEE Global Commun. Conf. (GLOBECOM'89)*, 1989, pp. 1680–1686.
[11] R. Gallager, "Low-density parity-check codes," *IRE Trans. Inf. Theory*, vol. 8, no. 1, pp. 21–28, 1962.
[12] K. R. Narayanan, "Effect of precoding on the convergence of turbo equalization for partial response channels," *IEEE J. Sel. Areas Commun.*, vol. 19, no. 4, pp. 686–698, 2001.
[13] S. Ten Brink, "Convergence behavior of iteratively decoded parallel concatenated codes," *IEEE Trans. Commun.*, vol. 49, no. 10, pp. 1727–1737, 2001.
[14] U. U. Fayyaz and J. R. Barry, "Polar code design for intersymbol interference channels," in *Proc. IEEE Global Commun. Conf. (GLOBECOM'14)*, 2014, pp. 2357–2362.
[15] M. Franceschini, G. Ferrari, and R. Raheli, "EXIT chart-based design of LDPC codes for inter-symbol interference channels," in *Proc. IST Mobile Summit*, 2005.
[16] L. Kong, Y. L. Guan, J. Zheng, G. Han, K. Cai, and K.-S. Chan, "EXIT-chart-based LDPC code design for 2D ISI channels," *IEEE Trans. Magn.*, vol. 49, no. 6, pp. 2823–2826, 2013.
[17] L. L. McPheters, S. W. McLaughlin, and K. R. Narayanan, "Precoded prml, serial concatenation, and iterative (turbo) decoding for digital magnetic recording," *IEEE Trans. Magn.*, vol. 35, no. 5, pp. 2325–2327, 1999.
[18] A. Morello and V. Mignone, "DVB-S2: The second generation standard for satellite broad-band services," *Proc. of the IEEE*, vol. 94, no. 1, pp. 210–227, 2006.
[19] J. R. Barry, B. Vasić, M. Khatami, M. Bahrami, Y. Nakamura, Y. Okamoto, and Y. Kanai, "Optimization of bit geometry and multi-reader geometry for two-dimensional magnetic recording," *IEEE Trans. Magn.*, vol. 52, no. 2, pp. 1–7, 2016.

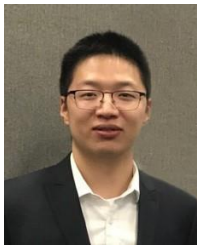

Shanwei Shi (S'18) received the B.S. degree in information engineering from Beijing Institute of Technology, Beijing, China in 2015. He is currently pursuing the Ph.D. degree in electrical and computer engineering with the Georgia Institute of Technology, Atlanta, GA, USA. He did internship in Seagate Technology, Shakopee, MN, USA in 2017. His current research interests are in the area of signal processing and communication theory, including equalization, detection, and coding as applied to magnetic recording channels.

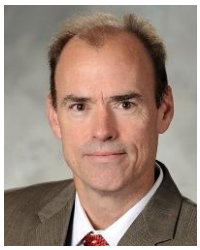

John R. Barry (SM'04) received the B.S. (*summa cum laude*) degree from the University at Buffalo, The State University of New York, Buffalo, NY, USA, in 1986, and the M.S. and Ph.D. degrees from the University of California at Berkeley, Berkeley, CA, USA, in 1987 and 1992, respectively, all in electrical engineering. His Ph.D. research explored the feasibility of broadband wireless communications using diffuse infrared radiation. He is currently a Professor with the School of Electrical and Computer Engineering, Georgia Institute of Technology. He has held engineering positions in communications and radar systems with Bell Communications Research, Murray Hill, NJ, USA, the IBM Thomas J. Watson Research Center, Yorktown Heights, NY, USA, Hughes Aircraft Company, Glendale, CA, USA, and General Dynamics Company, Falls Church, VA, USA, since 1985. He has co-authored a book entitled *Digital Communication-Third Edition* (Kluwer, 2004), co-edited a book entitled *Advanced Optical Wireless Communication Systems* (Cambridge University Press, 2012), and authored a book entitled *Wireless Infrared Communications* (Kluwer, 1994). He currently serves as a Guest Editor of the special issue of the IEEE JOURNAL ON SELECTED AREAS IN COMMUNICATIONS. He was a recipient of the David J. Griep Memorial Prize in 1992, the Eliahu Jury Award from the University of California at Berkeley, the Research Initiation Award from National Science Foundation, and the IBM Faculty Development Award in 1993.